CUADERNOS DE CAMPO DEL CUATERNARIO, Nº 3

AEQUA Field-Guide Series, Vol. 3

C3

QTEC-AEQUA

2016

Quaternary Tectonics in the Huercal-Overa and Eastern Basins of Almería (Eastern Betic Cordillera, SE España)

4th FIELD TRIP OF THE QTECT-AEQUA WORKING GROUP – October 2016

Antonio Pedrera (IGME)

Carlos Martín Lechado (IGME)

GRUPO DE TRABAJO DE TECTÓNICA CUATERNARIA, PALEOSISMOLOGÍA y ARQUEOSISMOLOGÍA - AEQUA

ASOCIACIÓN ESPAÑOLA PARA EL ESTUDIO DEL CUATERNARIO - AEQUA

Publication supported by the research projects "Tectonic map of the Iberian Peninsula and the surrounding cordilleras" and DAMAGE CGL2016-80687-R.

Cuadernos de Campo del Cuaternario

Guías de Campo de la Asociación Española para el Estudio del Cuaternario
AEQUA Field-Guide Series

ISSN-electrónico: **2386-8341**

Fotografía portada: La Molata Contractional structure near Albox, Huercal-Overa Basin, (A. Pedrera, 2016)

Autor de la fotografía / imagen: Antonio Pedrera (Instituto Geológico y Minero de España)

Se recomienda citar las partes de esta obra de la siguiente forma:
Pedrera, A., Martín Lechado, C. (2016). Título de la parada. En: Quaternary tectonics in the Huercal-Overa and Eastern basins of Almería (Eastern Betic Cordillera, SE Spain). ***C³ Cuadernos de Campo del Cuaternario***, 3. pp 7-8.

Edición y Maquetación:
Asociación Española para el Estudio del Cuaternario (AEQUA)
Escuela Politécnica Superior de Ávila (USAL).
Hornos Caleros, 50. 05003-Ávila, ESPAÑA
URL: www.aequa.es
e-mail: aequa@usal.es

Cuadernos de Campo del Cuaternario (C³) es una **iniciativa editorial AEQUA** que pretende recopilar todas las actividades de campo ligadas a los grupos de trabajo de la asociación, así como a los congresos y reuniones científicas que esta organice o en las que colabore.

Editores de la Serie: Pablo G. Silva y Pedro Huerta (Departamento de Geología, Universidad de Salamanca)

Autores Vol. 3: Antonio *Pedrera, Carlos Martín Lechado.*

Título Vol. 3: *Quaternary tectonics in the Huercal-Overa and Eastern basins of Almería (Eastern Betic Cordillera, SE Spain). En Inglés.*

Congreso / Reunión: *IV Reunión de Campo del Grupo de Trabajo QTECT-AEQUA. Almería 21 – 22 Octubre 2016.*

Agradecimientos / Acknowledgements Vol 3 (2016): W*ork supported by project "Tectonic map of the Iberian Peninsula and the surrounding cordilleras" and the MINECO Spanish Research Project DAMAGE CGL2016-80687-R.*

IV REUNIÓN DE CAMPO DEL GRUPO DE TRABAJO QTECT - AEQUA. ASOCIACION ESPAÑOLA PARA EL ESTUDIO DEL CUATERNARIO. ALMERÍA. OCTUBRE, 2016

Quaternary tectonics in the Huercal-Overa and Eastern basins of Almería (Eastern Betic Cordillera, SE Spain)

Tectónica Cuaternaria en las cuencas de poniente y Huércal-Overa (Cordillera Bñetica Oriental, SE Espña)

INDICE / INDEX.

C³

Cuadernos de Campo del Cuaternario

Vol 3 (2016). AEQUA

Quaternary Tectonics in the Huercal-Overa and Eastern basins of Almería (Eastern Betic Cordillera, SE Spain)

Edited by

A. Pedrera (IGME), C. Martín Lechado (UGR)

Other Authors

J.V. Pérez-_ Peña (UGR)

Introduction and Itinerary

A. Pedrera. *Instituto Geológico y Minero de España (IGME).* a.pedrera@igme.es
C. Marín-Lechado. *Instituto Geológico y Minero de España (IGME).* c.marin@igme.es

This field-trip is organized in the framework of the collaboration of the AEQUA Working Group on Quaternary Tectonics, Paleseismology and Archaeoseismology and IBERFAULT. Previous field-trips of QTECT-AEQUA were conducted in the Galera- Baza area (Granada; Garciá Tortosa et al, 2012), in ancient Roman city of Baelo Claudia (Cádiz; Silva et al., 2013), and in the Eastern Betic Shear Zone and the Aguilas Arc (Almería and Murcia; Silva et al., 2014)

The field-trip is designed to recognize the main tectonic structures that deform the Quaternary sediments in the Poniente and Huércal-Overa basins, to describe their recent evolution, their incidence in the topography, as well as to discuss their possible relation with seismicity.

The first journey was specifically focused on the Poniente Basin, in the Campo de Dalías that is deformed by ENE-WSW open folds and NW-SE / WNW-ESE normal-oblique faults.

The folds controlled the basin evolution from the upper Miocene and, at present, they have a clear incidence in the topography. The faults are nucleated on previous joints and propagated during the late Pleistocene and Holocene. The Campo de Dalías and adjacent sectors represent an area with a high relative concentration of major earthquakes (Mw 5.0-6.5) with recurrent events in 1804, 1910 and 1994.

The second journey will visit the western part of the Huércal-Overa basin. Reverse faults and folds that interacted with the drainage network will be recognized. Although these structures show evidences of a progressive evolution at low deformation rate, some historic earthquakes have occurred in this sector and could be associated with their activity (e.g. the Partaloa earthquake in 1972, mbLg 4.8 and intensity VII).

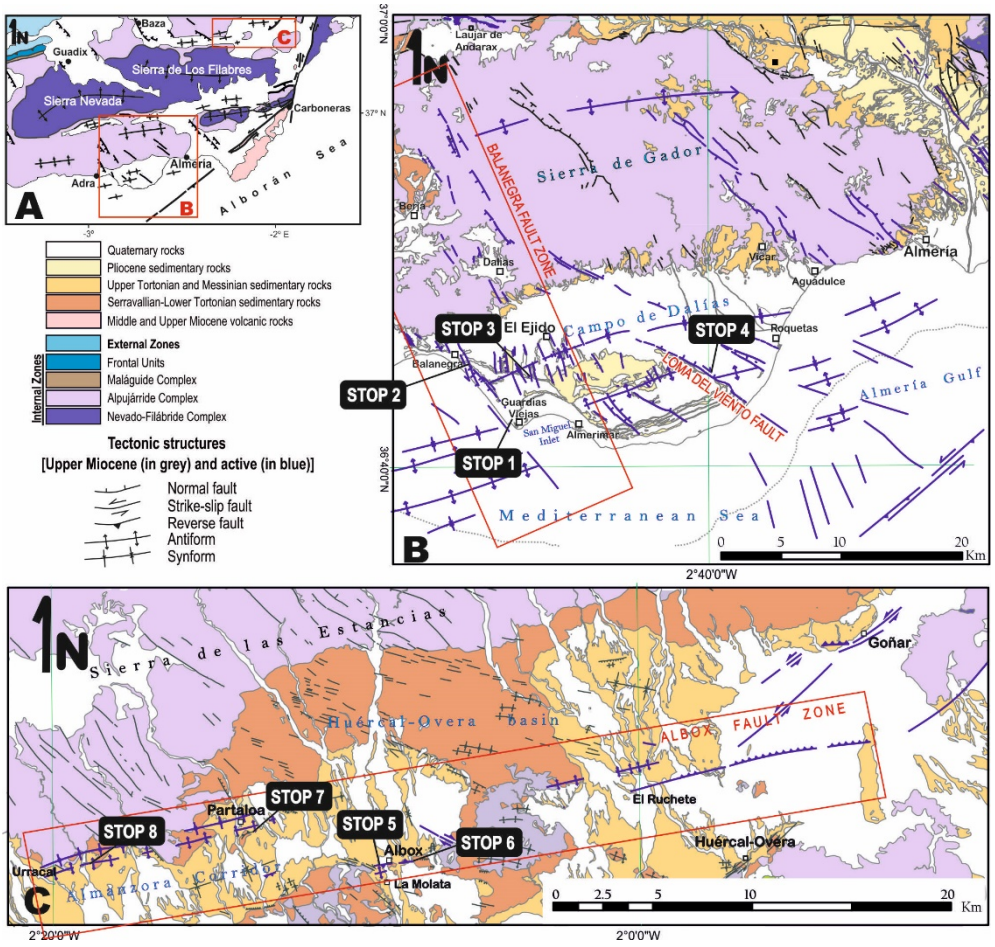

Fig. 0.1. Geological maps and field-trip stops during days one and two. (A) Geological map of the central-eastern Betic Cordillera. (B) Geological maps of the Poniente Basin in the Campo de Dalías (C) and the Huercal-Overa Basin. The stops described below are marked. The traces of the recent (in grey) and active (blue) tectonic structures are highlighted (Modified from Pedrera et al., 2012).

Geologic and geodynamic setting

A. Pedrera. *Instituto Geológico y Minero de España (IGME). a.pedrera@igme.es*
C. Marín-Lechado. *Instituto Geológico y Minero de España (IGME). c.marin@igme.es*

The recent and active tectonic structures of the Betic Cordillera have attracted attention of Earth scientists since the 1970s (e.g. Andrieux et al., 1971; Groupe de Recherche Neotectonique, 1977; Bousquet, and Montenat,1974; Bousquet and Phillip, 1976), and since then, much geological and geomorphologic research has been focused on their identification in order to establish the mechanisms responsible for the tectonic evolution of the orogen and to estimate their seismogenic potential (e.g. Sanz de Galdeano and Lopez Casado, 1988; Sanz de Galdeano et al., 1995).

This region exhibits a variety of deformational styles, dominated by folds, right-lateral and normal faults in the central Betics (e.g. Galindo-Zaldívar et al., 2003), and by large left-lateral strike-slip faults in the eastern sector of the cordillera that also interact with folds and normal/normal-oblique faults (e.g. Martínez-Díaz, 2002; Masana et al., 2004; Booth-Rea et al., 2003; Pedrera et al., 2010) (Fig. 0.2). The present field trip attempts to show some of the most striking Quaternary tectonic structures that deform the Poniente and the Huércal-Overa basins, both placed in the Internal Zones of the orogen (Figs 0.1 and 0.2).

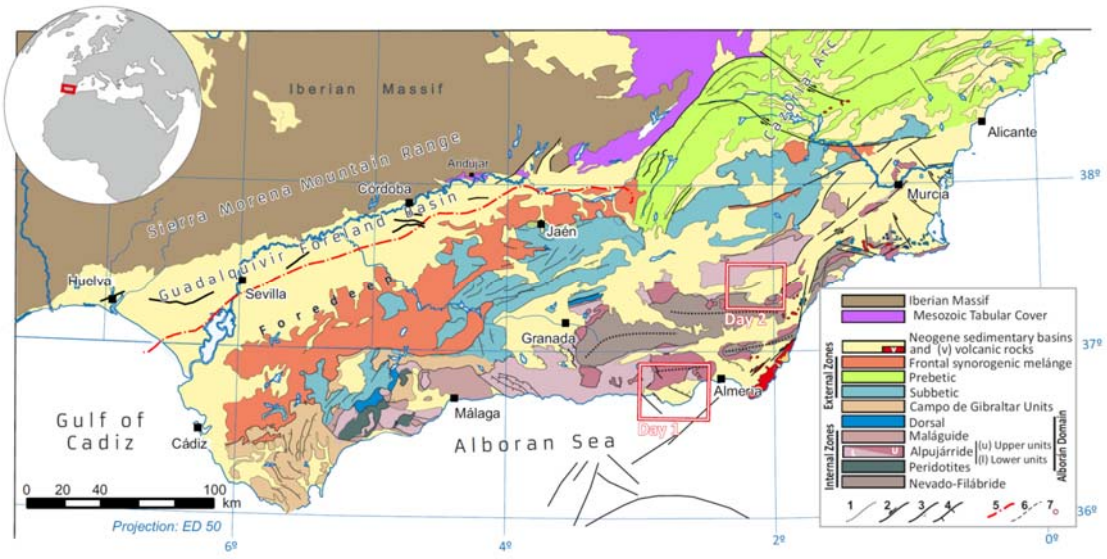

Fig. 0.2. Simplified geological map of the Betic Cordillera showing the location of the Poniente and the Huércal-Overa basins (Modified from Marín-Lechado et al., 2017).

The Betic Cordillera, which is connected with the Rif across the Gibraltar Tectonic Arc, is the westernmost termination of the Alpine Mediterranean belt (Figs. 0.2 and 0.3A). Its formation was driven by the NW-SE to N-S convergence between the major Iberian and African plates, which interacted with the relative westward displacement of the Alborán Domain (e.g. Sanz de Galdeano, 1990). Mesozoic oceanic crust and the contiguous thinned continental crust of the South Iberian and North Maghrebian paleomargins were subducted beneath the Alborán continental lithosphere between the late Oligocene and the middle Miocene (e.g., Lonergan and White, 1997). Roll-back of this E to SE-dipping subducted oceanic slab favored the collision of the Alborán Domain with the paleomargins (e.g. Pedrera et al., 2011) (Fig. 0.3B). Frontal thrusting and extension at the rear were coeval (e.g. Platt et al., 2003).

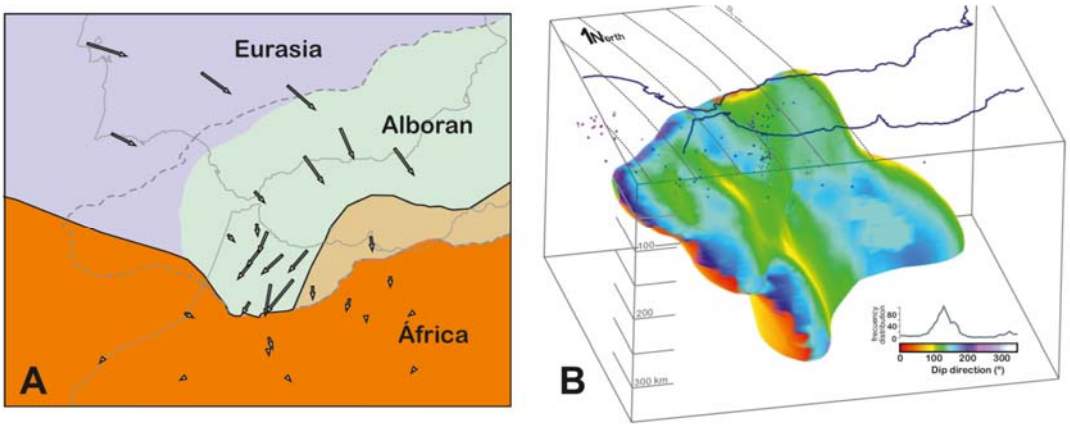

Fig. 0.3. Present-day geodynamic setting in the western Mediterranean (Modified from Pedrera et al., 2011). A. Proposed plate boundary between the Eurasian and Africa plates in the western Mediterranean and GPS velocity field considering Africa fixed. Note that the eastern Rif, marked in light orange colour, behaves as a quasi-rigid block welded to the stable African plate. B. Three-dimensional reconstruction of positive seismic velocity anomaly detected beneath the Gibraltar Arc from available tomographic images of P-wave velocity anomalies that could be interpreted as subducted lithosphere. The intermediate seismicity, the SHmax trajectories, and has been also plotted.

Subduction shifted to N-S/NW-SE continental collision roughly since late Serravallian, as a consequence of the high mechanical coupling between the Alborán and the Iberian colliding plates (Pedrera et al., 2013; Marín-Lechado et al., 2017). This continent collision is still active at a rate of 4-5 mm/yr and drives the development of active folds and faults. Current GPS displacement reveals the oblique convergence between the Iberian and African plates, showing a movement of the Eurasian plate and the Betic Cordillera toward the SSE/SE with respect to the African plate (e.g. Vernant et al., 2010), which is roughly in accordance with the present-day stress setting (e.g., Pedrera et al., 2011) (Figs 0.3). Seismological data reveal a low to moderate seismicity with a broad distribution (e.g., IGN 2008). Earthquake focal solutions obtained in the Eastern Betics support coeval NW-SE compression and orthogonal extension.

Stop 1: Castillo de Guardias Viejas. Overall tectonic structure of the Poniente Basin and the Guardias Viejas antiform

C. Marín-Lechado. *Instituto Geológico y Minero de España (IGME). c.marin@igme.es*
A. Pedrera. *Instituto Geológico y Minero de España (IGME). a.pedrera@igme.es*

The Poniente Basin is located at the boundary between the Alborán Sea and the Betic Cordillera, in the so-called Campo de Dalías. Tortonian and Pliocene marine sedimentary rocks, which belonged to the Northern Alborán basin, have emerged in Quaternary times.

The northern margin of the Alborán Sea and the onshore Campo de Dalías are deformed by an 80 km-long set of anticlines and synclines trending ENE–WSW (Fig. 1.1) (Baena et al.,1982; Comas et al., 1992; Pérez-Belzuz, 1999; Rodríguez-Fernández and Martín-Penela, 1993; Vázquez, 2001). The folds have been interplaying with sedimentation since late Miocene time. A synform- antiform pair is identified in the basin and referred as Ejido Synform and Guardias Viejas Antiform. Alpujárride rocks crop out along the antiform trace in the Guardias Viejas castle sector, the stop 1 (Marín-Lechado et al., 2006; Pedrera et al., 2015).

The Guardias Viejas antiform started to grow in late Tortonian as two isolated segments (A and B) separated by an antiformal saddle zone (Fig. 1.1). Between ~7.5–8 and 7.2 Ma, they were isolated fold segments. During Messinian times, the growing topography associated with the Guardias Viejas antiform induced a trapping of sediments in the northward synform. This prolonged syn-deformation process would have caused the development of a progressive unconformity in the basin margins with basinward progradation. The three-dimensional shape of the Messinian layer, together with its thickness and internal unconformities, reveal lateral propagation of the two antiform segments (A and B, until linkage). The maximum average shortening during late Tortonian and Messinian times coincides with these two segments (Fig. 1.1).

After linkage of the two antiform segments, both the Guardias Viejas Antiform and the Ejido Synform continued growing symmetrically while accommodating maximum shortening in the saddle sector. Thus, the growing topography related to antiform amplification affected the sedimentation of Pliocene and Quaternary units. Therefore, alluvial fan deposit from the nearby Sierra de Gádor was restricted to the north of the antiform. It is important to note that although the normal-oblique faults have associated marked topographic scarps, they did not control the upper Miocene and Pliocene sedimentary depocenters. Actually, these normal-oblique faults formed subsequently in Quaternary times and their offsets range from a few meters to several tens of meters.

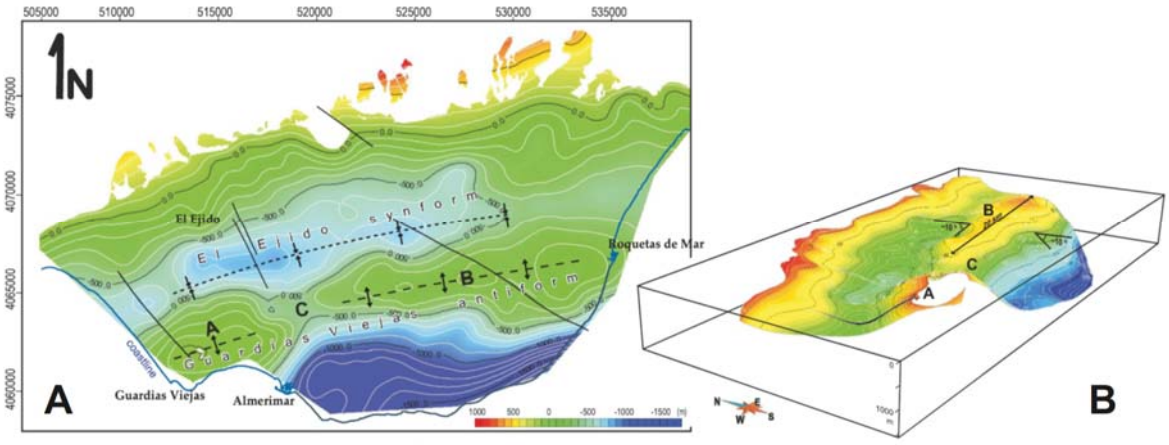

Fig. 1.1. Top of the basement (pre-growth surface). (A) Contour map of the Alpujarride top surface. The trace of the folds and faults is marked. Two segments along the Guardias Viejas Antiform (A and B) where the folded Alpujárride top reaches maximum heights, are separated by an antiformal saddle sector (C). (B) 3D view of the folded upper Tortonian bottom (Vertical exaggeration ×3) (Modified from Pedrera et al., 2015).

Stop 2: Calle Las Cuevecillas – Cta. de Las Salinas (Norte de Balerma).
Tectonics and Geomorphology of the Balanegra Fault zone

C. Marín-Lechado. *Instituto Geológico y Minero de España (IGME). c.marin@igme.es*
A. Pedrera. *Instituto Geológico y Minero de España (IGME). a.pedrera@igme.es*

After the Pleistocene, WNW–ESE and NNW–SSE trending normal and oblique normal faults started to develop coeval with the folds in the Poniente Basin (Figs. 2.1 and 2.2). The maximum fault offsets range from few meters to several tens of meters, and they have associated marked topographic features. The kinematics of the faults range from normal-dextral to normal-sinistral and they have associated small to moderate earthquakes (e.g. Marín-Lechado et al., 2004, 2005; Pedrera et al., 2012).

The Balanegra Fault Zone is one of the most prominent fault in the Poniente Basin, formed by southwestward dipping fault segments trending NW–SE, which extends from the north of Berja towards the Alborán Sea, controlling the western end of the Sierra de Gador antiform and the NW–SE oriented straight morphology of the coastline (Marín-Lechado et al., 2004, 2005; Galindo-Zaldívar et al., 2013). A seismic series occurred along the BFZ in 1993–1994 (Fig. 2.1C).

Fault slip rate values estimated in the fault segment that limits the western border of the Sierra of Gádor are comprised between 0.1 and 0.3 mm/year (Martínez-Díaz and Hernández-Enrile, 2004), in the northern part of Balanegra Fault Zone. Westward, Gràcia et al. (2012) identify the NW–SE trending Adra Fault that extends 20 km offshore, reaching the seafloor surface (Fig. 2.1). The NW–SE oriented, westward-dipping Balanegra Fault Zone (Figs. 2.1 and 2.2) is an active fault zone, as can be inferred from its syn-tectonic Quaternary deposits, its evident topographic escarpment in the landscape, and its associated seismic activity (Fig. 2.2C). Outcropping fault surfaces are only found near the village of Balanegra, where N160 ^{o}E/75 ^{o}W fault segments crop out with slicken lines plunging 70^{o}S. Southwards, the Balanegra Fault Zone gives rise to a 6-km-long N140 ^{o}E oriented lineament parallel to the coastline, where the difference in topography associated with fault activity is of about 45 m, and Pliocene sediments have cross-bedding laminations dipping up to 30 ^{o}towards the downthrown block. Offshore, high-resolution sea-floor imaging shows lineaments mainly parallel to the Balanegra Fault Zone with a mean trending of N140-145^{o}E (Gràcia et al., 2012). Thus, the BFZ is formed by a set of overstepping segments extending sea-wards, separating the eastward upthrown Campo de Dalías from the westward downthrown Alboran Sea. The vertical throw of the main onshore fault segment was determined by repeated measurements between 2006 and 2012 along two high precision levelling profiles. The vertical throw of the main onshore fault segment was determined by repeated measurements between 2006 and 2012 along two high precision levelling profiles. The fault shows a ~0.4 mm/year mean rate of deformation in the period comprised between major earthquakes with a very complex behavior.

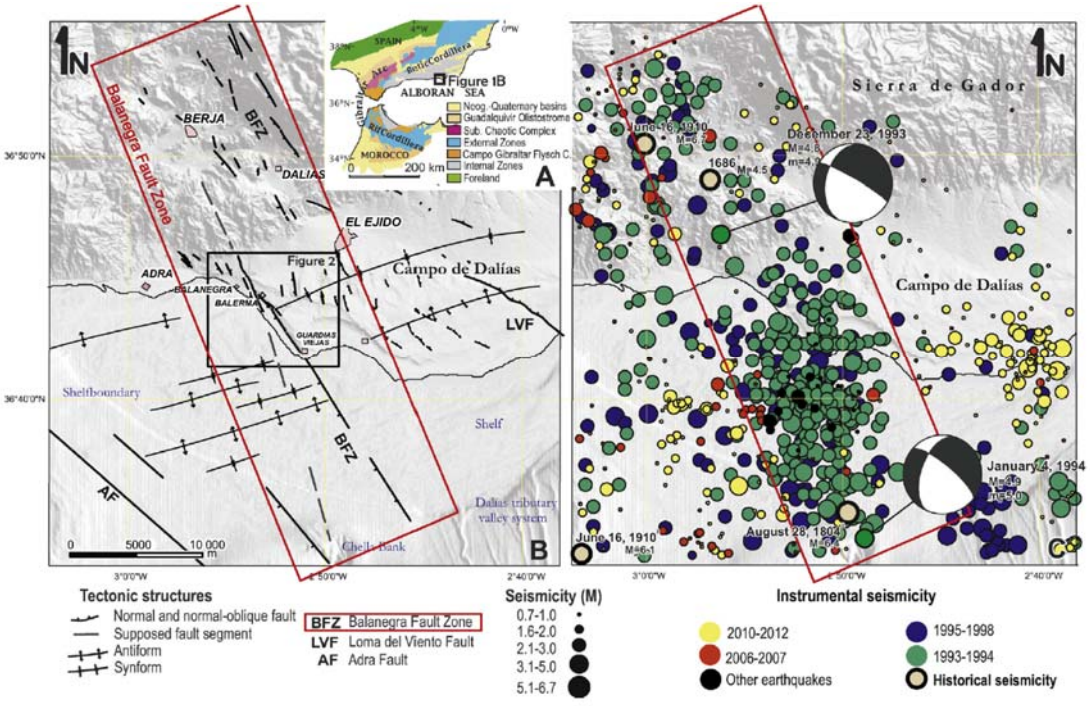

Fig. 2.1. Geological setting of the study area. (A) Regional geological setting. (B) Digital elevation model with faults (black lines) recognised on field and lineaments offshore from slope gradient. (C) Seismicity within and near Balanegra Fault Zone. The aftershocks of the 1993–1994 series, seismicity from 1994 to 1998, the cluster of microseismicity of 2006–2007 and the seismic period of 2010–2012 are differentiated (Galindo-Zaldívar et al., 2013)

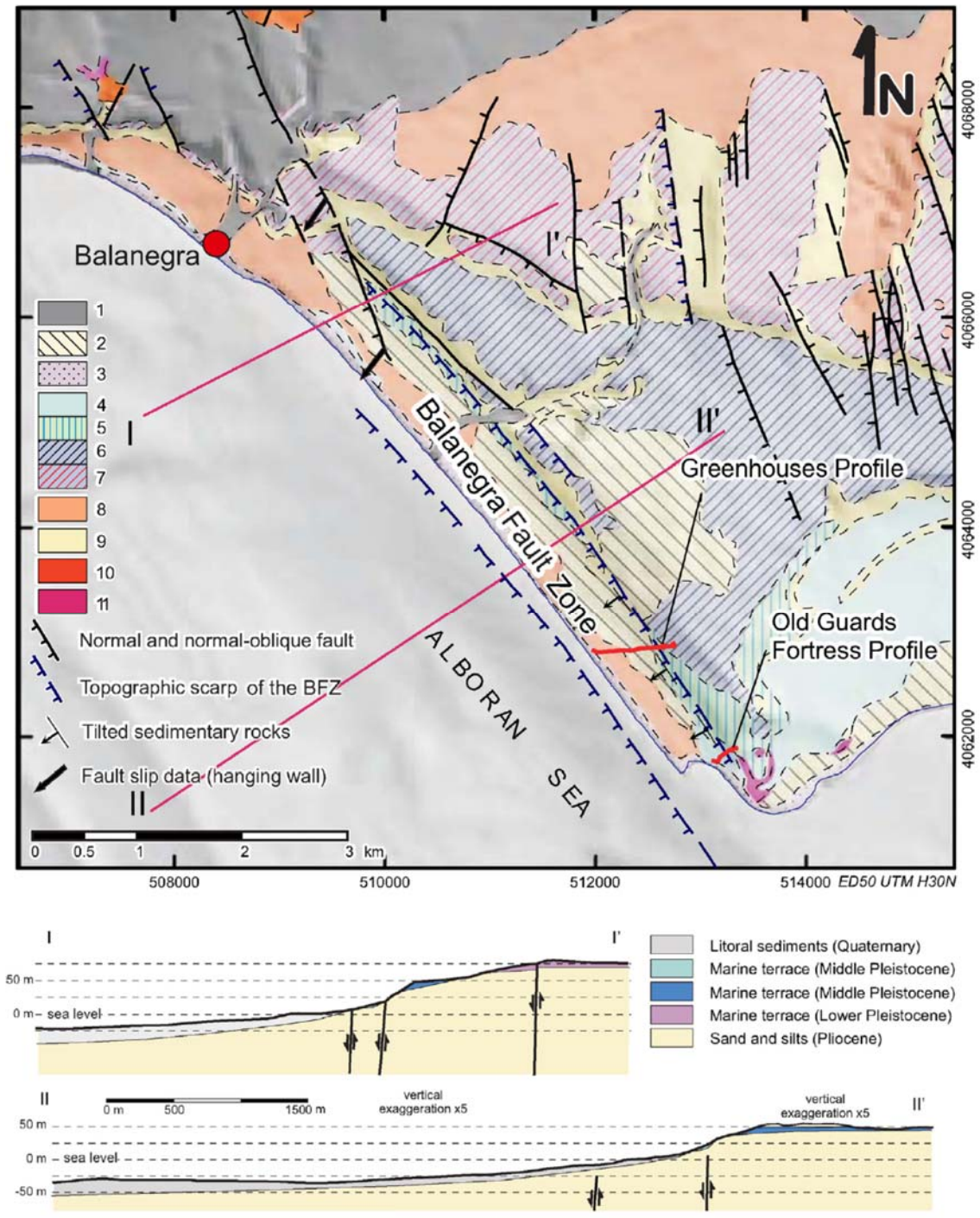

Fig. 2.3. Geological map of Balanegra Fault Zone (Galindo-Zaldívar et al., 2013). Levelling profiles (red lines). Legend: 1 – Alluvial deposits (Holocene), 2 – Dunes (Holocene), 3 – Beach deposits (Holocene),4 – Marine terrace (Upper Pleistocene), 5 – Marine terrace (Middle Pleistocene), 6 – Marine terrace (Middle Pleistocene), 7 – Marine terrace (Lower Pleistocene), 8 – Reddish silts (Pleistocene), 9 – Sands and silts (Pliocene), 10 – calcarenites (Upper Tortonian), 11 – Limestones and dolomites (Alpujárride basement). Topographic data extracted from a 10 m resolution Digital Terrain Model (Junta de Andalucía, 2005).

Stop 3: Cantera de Matagorda. Faulted joints in the Matagorda quarry

C. Marín-Lechado. *Instituto Geológico y Minero de España (IGME). c.marin@igme.es*
A. Pedrera. *Instituto Geológico y Minero de España (IGME). a.pedrera@igme.es*

Pliocene calcarenites exposed in the Matagorda Quarry allowed the geometry and distribution of Pliocene joints to be detailed studied on a horizontal plane (Fig. 3.1). A plot of the joint trends against their cumulative length shows that more than 80% of all joints trend between N140ºE and N170ºE, with a maximum at N160ºE. The joints of greater length (belong to a well-defined joint spectrum with orientations ranging from N145ºE to N165ºE. The angle between the two joint sets that define the extremes of the joint spectrum ranges from 20 to 25º. Outcrop-scale joint patterns show indentation of rock wedges bounded by two joint sets, with X and Y geometries and defining variable opening directions of the joints (Fig. 3.2). In general, the amount of opening is smaller for two pairs of joints meeting at acute angles than for single joints with intermediate orientation. Upper Pleistocene-Holocene sediments seal the joint spectrum of the Matagorda outcrop (Fig. 3.2).

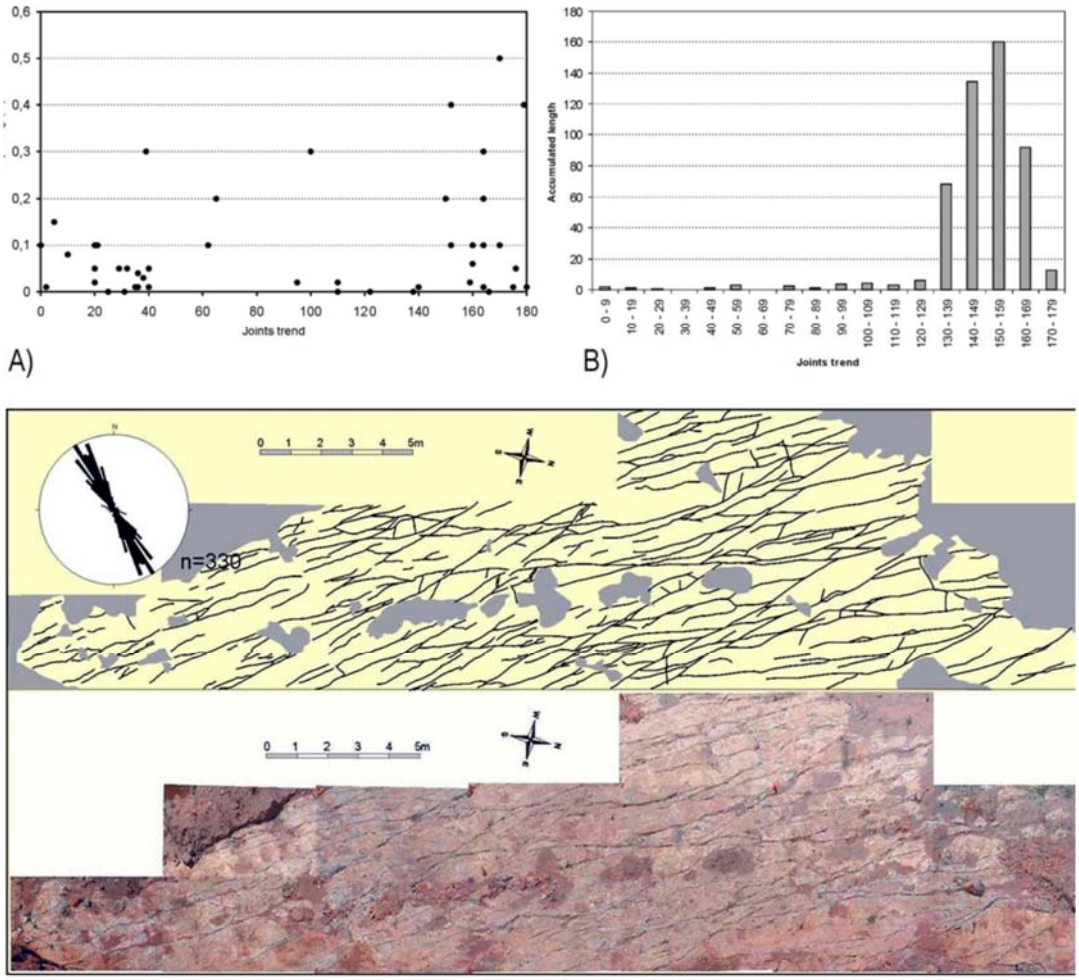

Fig. 3.1. Example of hybrid and tensional joints constituting a joint spectrum in the Campo de Dalias (Marín-Lechado et al., 2004). (A) Opening versus joint trend. (B) Accumulated length (m) versus joints trend. (C) Detailed photo mosaic and sketch in plan-view, showing the distribution pattern of joints in Matagorda Quarry.

However, some Pliocene joints acted as planes of weakness along which faults developed. The impressive faults in the Matagorda Quarry have nearly vertical fault planes that feature upper Pleistocene–Holocene activity, evidenced by the development of sedimentary wedges of variable polarities (Fig. 3.2D). Faults use preexisting joints as easy-slip planes and could be defined as faulted joints (Wilkins et al., 2001). Subvertical joints and faults show similar patterns at outcrop scale and in aerial photographs. The fault distribution with angles in-between of 30º in map view is quite similar to the attitude of joints at outcrop scale defining joint spectra. The fault slip is generally oblique, as a function of initial joint orientation, they show normal-dextral or normal-sinistral depending on the initial joint orientation.

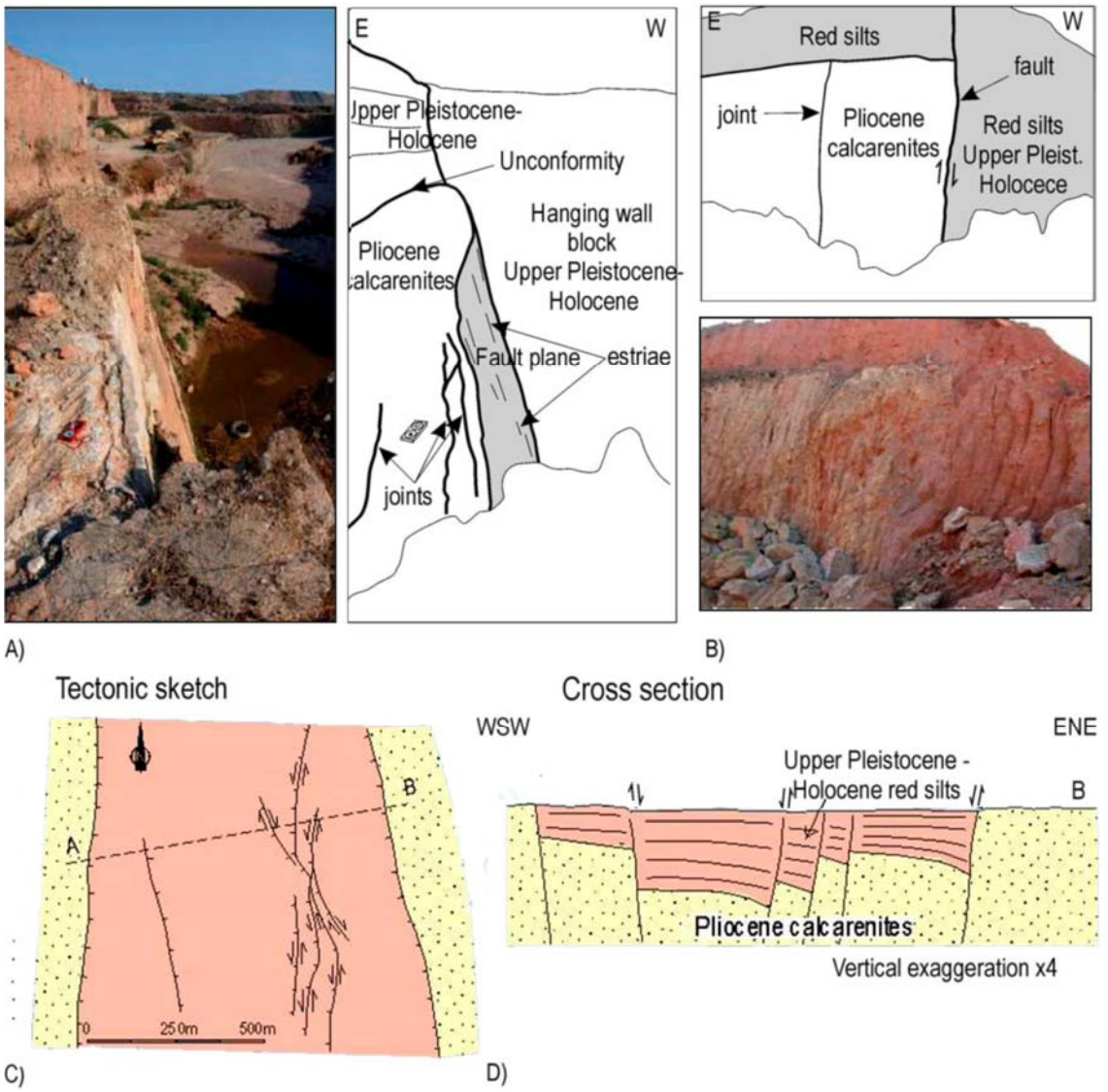

Fig. 3.2. Faulted joints and related structures in Matagorda Quarry (Marín-Lechado et al., 2004). (A and B) Joints parallel to faulted joints in Pliocene calcarenites. Note the presence of an unconformity between Pliocene and Upper Pleistocene–Holocene rocks. (C) Tectonic sketch of Matagorda Quarry showing the fault pattern and its similarity with the joint pattern at outcrop scale. (D) Cross-section of Matagorda Quarry with the development of a half graben structure during Late Pleistocene–Holocene.

Stop 4: El Solanillo (Cantera Cta. San Agustin). The Loma del Viento Fault

C. Marín-Lechado. *Instituto Geológico y Minero de España (IGME). c.marin@igme.es*
A. Pedrera. *Instituto Geológico y Minero de España (IGME). a.pedrera@igme.es*

The Loma del Viento fault covers over ~8 km of fault trace, extending from just west of La Mojonera village toward the continental shelf, with a N120ºE average strike (Fig. 4.1). In detail it is seen to be a segmented fault comprising six onshore hard-linked and soft-linked segments recognized by their average strike that varies between N105ºE and N135ºE, with sub-segments, steps, bends, and associated zones of contractional and extensional jogs. The average dip is 80º toward the NNE, though some sub-segments are vertical and others dip 80º toward the SSW. One of these fault segments, the so-called segment B, is well-exposed in El Solanillo sector. The features of each segment are described from northwest to southeast.

- Segment 0 is a 2500 m long, N110ºE-oriented, morphologically well-defined scarp where no fault segments are observed (Fig. 4.1). It would be related to the upward propagation of a fault segment with a normal component that does not reach the topographic surface. The morphological scarp is enhanced from Las Norias village toward the south, reaching 40 m of maximum topographic scarp close to segment A.

- Segment A is a 1800 m long and 250 m wide fault zone formed by a N120ºE sub-segment dipping between 90º and 70º toward the NNE. Its kinematics, deduced from fault slickenlines, is dextral-normal with a rake of 30º-50º toward the ESE (Fig. 4.1). Penetrative joints deform Pliocene calcarenites close to the fault scarp. Some of these joints are faulted, showing an oblique-normal slip consistent with the kinematics of the main fault plane. It has an associated maximum topographic scarp of 38 m. Segments A and B are soft-linked, and develop an extensional overstep characterized by N170º-150ºE vertical faults with dip-slip and 80º W-dipping faults with oblique left-lateral slickenlines.

- Segment B is a narrow fault zone, measuring just a few meters, formed by three main parallel sub-segments that stretch over 1000 m and have a N135ºE strike with a dip from 70º to 90º toward the northeast. The rake of the slickenlines varies between 15º and 45º toward the ESE, revealing a dextral-normal behavior. The interaction between the three parallel sub-segments produce contractional oversteps resolved by N90ºE pure dextral faults that transfer the offset between them and N70ºE tight folds. Pleistocene red sands, silts and clays are placed in the hanging wall associated with the fault activity (Fig. 4.1). The segments B and C are hard-linked into a joined curved fault surface that slips together, as deduced from the 22 m of maximum topographic scarp (Fig. 4.1). Therefore, the maximum thickness of the Pleistocene sedimentary unit (90 to 100 m), which represents a syn-fault deposit, occurs along this linking sector.

- Segment C runs 1200 m with a N105ºE average strike, and generally dips 90º to 70º towards the NNE. However, some sub-segments dip 80º toward the SSW along tens of meters, showing a reverse fault component. The kinematics of this sector of the Loma del Viento fault are quite constant with the rake of the slickenlines of 40º toward the ESE and dextral-normal regime. We recognized an extensional overstep between segments C and D, which is characterized by N150ºE oriented conjugated normal faults with ~200 m long fault traces (Fig. 4.1B).

- Segment D is formed by two main sub-segments oriented N120ºE, the total length of the segment being 1000 m (Fig. 4.1). Both sub-segments have dextral-normal kinematics, while the linking sector between them is a contractional overstep characterized by N90ºE to N130ºE reverse-sinistral faults. The topographic scarp associated with the fault activity grows toward the southeast, reaching 17 m near the linking sector between faults D and E (Figs. 4.1). Marine conglomerates and sands belonging to the topographically higher Pleistocene marine terrace were deposited in the fault hanging wall.

Long-term slip rate

The detritic unit composed of red sands, silts and clays was coevally deposited during the movement of fault segments B and C. Its maximum thickness coincides with the hard-linkage sector between these two segments. The fault linkage enhanced the slip and controlled sedimentation. This sedimentary unit has a wedge geometry thickening as much as 90 to 100 m toward the fault plane. A Pleistocene age is assigned to these sediments based on their stratigraphic position —unconformable above Lower to Middle Pliocene marine sedimentary rocks. On the basis of estimated maximum thickness, estimated age of the deposits, dip of the fault plane, and the 40º oblique-slip deduced from the fault slickenlines, the slip rate in the central part of the Loma del Viento fault was assessed. This estimation is hampered by some uncertainty entailing constraints on age and sedimentary thickness. Hence, we evaluate the min/max age of the formation (~3.6 to ~1.8 Ma) and calculate a min/max fault off-set (90 to 100 m). We thus arrived at a long-term slip rate of 0.07 ± 0.03 mm/y.

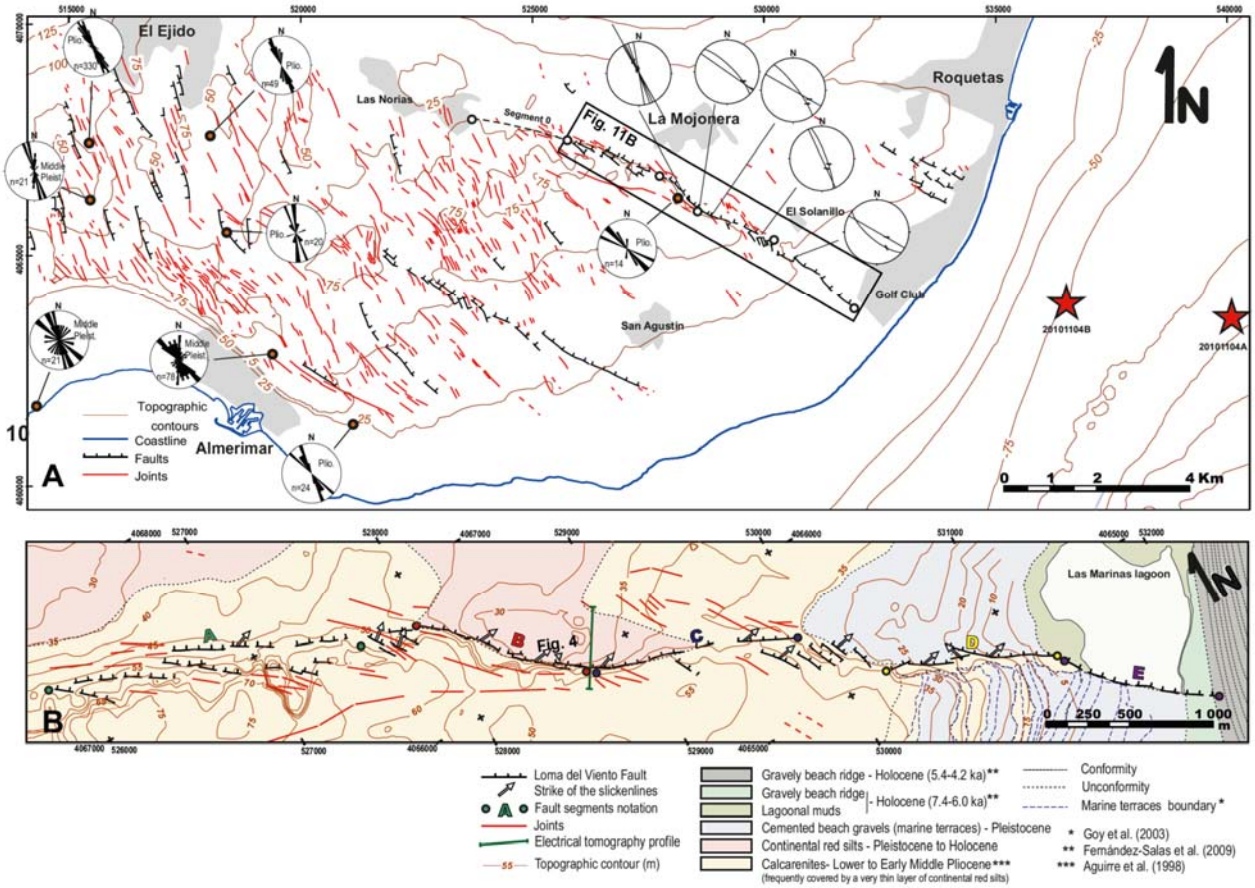

Fig. 4.1 The Loma del Viento Fault (Modified from Pedrera et al., 2012). A. Tectonic map of the Campo de Dalías with location of main joints and main faults. Rose diagrams of joints from several measurement sites. The number of data is indicated by the lower number (n). Age of sediments is included in each measurement station. In addition, rose diagrams of all the joints and fault segments mapped using aerial photographs are included. Stereoplots (lower hemisphere) of fault planes and striae in the Loma del Viento fault are also included. The epicenters of the two major earthquakes with magnitude (Mw) 3.5 and 4.2 that occurred in November–December 2010 close to the southern termination of the Loma del Viento fault are plotted. B. Detailed geological map of the Loma del Viento fault

.

Stop 5. Western Access to Albox by Cta.AL-831. La Molata Contractional structure (Albox Fault zone)

A. Pedrera. *Instituto Geológico y Minero de España (IGME). a.pedrera@igme.es*
C. Marín-Lechado. *Instituto Geológico y Minero de España (IGME). c.marin@igme.es*

Along the new road from Albox to La Molata there is a very well exposed compressive structure that includes reactivated Neogene faults, active reverse faults and associated active folds (Fig. 5.1). At its base, the outcrop shows a multilayer sequence, formed by centimetre-thick beds with alternating continental red conglomerates, sands and silts. These continental deposits grade into a various coloured sequence of conglomerates, sands, grey silts and caliches that probably developed in a shallow marine environment. These levels possibly belong laterally to the nearby stratigraphical section studied by Guerra-Merchán et al. (2001) and dated as Tortonian due to the presence of a micromammal site located in fluvial levels. At the top of this unit there is an angular unconformity (U1) and a thin deposit formed by conglomerates and a yellow sandy matrix. The age of these sediments is not well constrained, but could correspond laterally with early Messinian marls defined by Briend (1981) and recently dated by Meijninger (2006). Just at the top appears a new angular unconformity (U2) overlain by a lacustrine formation, harbouring a micromammal site, 'Albox1', assigned to a middle Pleistocene age (Pedrera et al., 2009).

At a large scale, the structure consists of a N-vergent disharmonic antiform that interacts with dextral-reverse and pure reverse faults. In the internal part, the antiform is closed and bounded by two high-angle transcurrent faults. The kinematics deduced from the gouges developed in these faults exhibit main dextral-reverse behaviour, although sinistral movements were also found. The orientation of the axis of this fold coincides with the dextral fault trends that vary between N145º E and N100º E. Transcurrent faults developed in multicoloured fault rocks where the relatively resistant blocks are surrounded by finely deformed gouges. Only two dextral-reverse faults are associated with the antiform that deforms the Pleistocene sediments and cuts the U1 (Fig. 5(B)). This antiform is N-vergent, has a N70º E orientation and is clearly synsedimentary with respect to the middle Pleistocene lacustrine deposits that have an internal unconformity (U3). The antiform is active at present, as we deduce from the topographic high. In addition, the lacustrine deposits are deformed by secondary south-dipping reverse faults that are N70º E oriented.

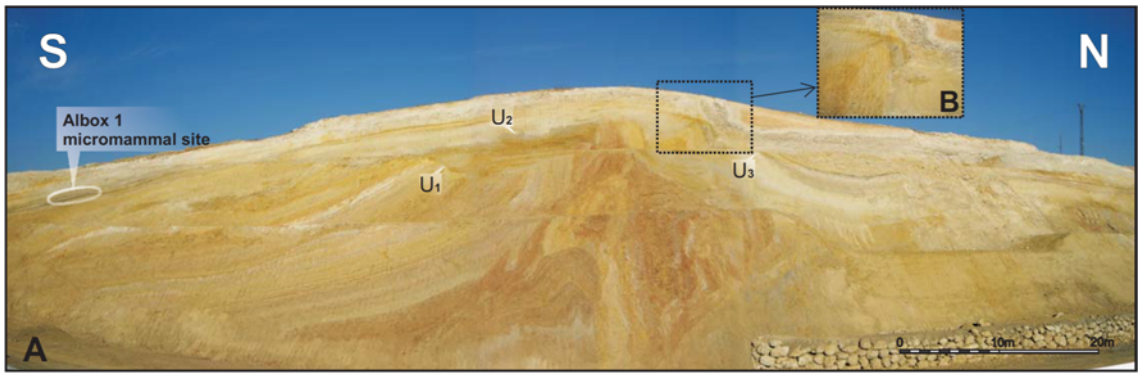

Figure 5.1. La Molata structure (Pedrera et al., 2009). (A) The unconformities and the Albox 1 micromammal site are plotted. Position of the outcrop is marked in figure 2. (B) Enlarged picture showing the two dextral-reverse faults that deform the unconformity 1 (U1) and are associated to the Quaternary antiform.

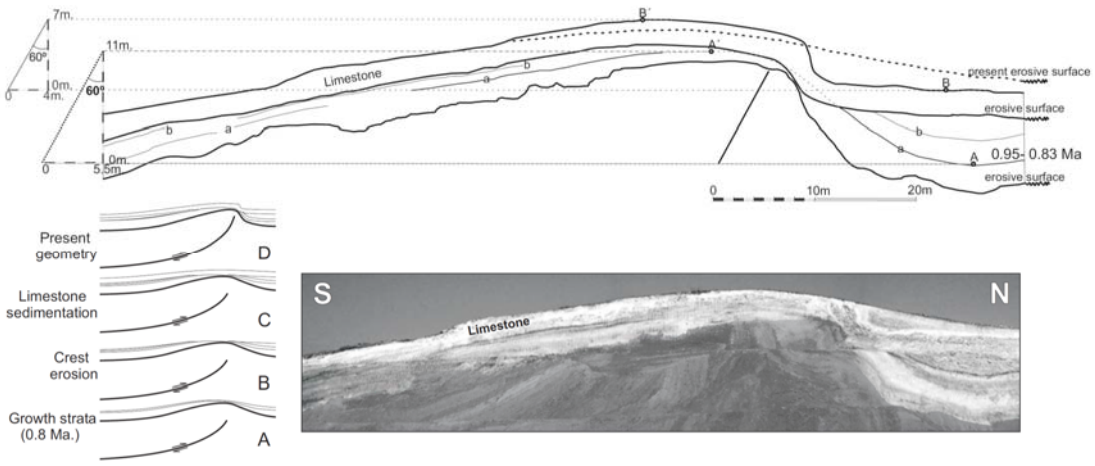

Figure 5.2. Tectonic evolution of the La Molata structure (Pedrera et al., 2009). (A) Strike-slip faulting with development of thick fault gouge, uplift, erosion and formation of the unconformity 1 (U1). (B) The old dipping faults zones are reactivated as reverse faults with associated folds that are coetaneous to the lacustrine Quaternary sediments deposition. (C) The Quaternary syn-tectonic sedimentation continues.

We can establish the deformation rate from the Middle Pleistocene up until now using the new biostratigraphical data and restoring the unconformities up to the horizontal. The model of Fig. 5.2 shows a general tectonic restoration. In a first stage (A), WNW–ESE dextral-reverse faults with associated wide fault gouge were active, prior to the U1 erosive unconformity. These precursory fault gouges constitute heterogeneities that favour the progression of deformation parallel to these weak sectors during the Quaternary. Stages B and C illustrate the development of reverse faults and associated antiforms.

The vergence to the north of the upper folds highly conditioned the accommodation space in both flanks, and causes the lacustrine sediments to become thicker in the northern flank. The Quaternary sedimentation was affected by the fold growth, giving rise to growth strata (Fig. 5.3). The folding is related to a northward-propagating N70º E oriented reverse fault dipping 55º S. We sequentially reconstructed the folding inferred from the syntectonic geometry of the growth strata, deducing a limb rotation of synclinal hinge during the development of the fold. The thin layer 'a', dated as Middle Pleistocene, and the footwall of the limestone layer 'b' were considered to determine the deformation rates and to establish the active fault dipping.

In these reference surfaces, the lowest (A, B) and highest (A´, B´) points were determined in order to establish the vertical offset of each layer. Horizontal shortening was determined by restoring the cross-section. We deduce that the deformation propagates over a 60º S dipping reverse fault, fitting quite well with the younger measured fault in the outcrop (55º S dip). Using layer 'a', containing fossils from 0.95–0.83 Ma, and taking into account that it was deposited during the first stage of the fold development, we obtain ~0.012–0.013 mm/y uplift and ~0.006 mm/y horizontal shortening rates.The rate deduced for the fault slip is ~0.014–0.016 mm/y. These deformation rates are similar to the rates suggested for the eastern Albox fault: 0.01–0.02 mm/y uplift rate and a 0.03 mm a-1 fault slip rate last for the last 63.3 ka (Masana et al., 2005).

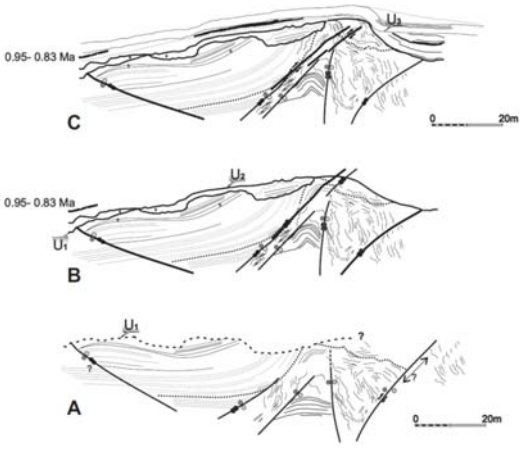

Figure 5.3. Restoration of the Quaternary fault-propagation fold in the La Molata structure (Pedrera et al., 2009) (A-D). We have restored up to the horizontal the 11 m of vertical displacement (point A-A´) in the layer "a" (0.95-0.83 Ma) obtaining 5.5 m of horizontal shortening. The same procedure for the limestone layer footwall ("b"): 7 m of vertical uplift and 4 m of horizontal shortening. In both cases the obtaining fault dip is 60º to the South.

Stop 6: Camino de Aljambra (Albox). Reverse faulting affecting to Pleistocene fluvial conglomerates (The Albox Fault Zone)

A. Pedrera. *Instituto Geológico y Minero de España (IGME). a.pedrera@igme.es*
C. Marín-Lechado. *Instituto Geológico y Minero de España (IGME). c.marin@igme.es*

Close to the town of Albox, several outcrops show small reverse faults and associated compressive structures deforming Quaternary fluvial sediments (Fig 6.1). The trends of these faults are between N70º E and N90º E, dipping indistinctly northwards and southwards between 20º and 40º, and sometimes up to 60º. The kinematics deduced from the striations located on the fault planes indicate pure reverse faulting when they are N70º E oriented, and reverse-dextral faulting when the orientation is close to E–W. These results are in agreement with the observations of Briend (1981) in the eastern part of the basin. When the sediments deformed by the fault zone are conglomerates, the pebbles are reoriented during the reverse slip.

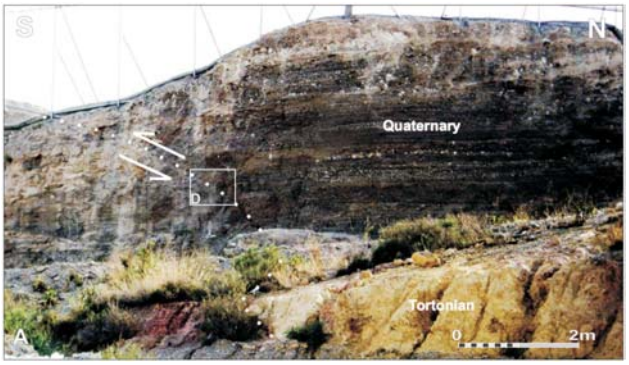

Fig. 6.1. Field example of reverse N70º E oriented fault that deforms the most recent Quaternary alluvial fan of the area.

Stop 7: Ctª. A-399 (South of Partaloa). Small scale active folds in the Partaloa-Urracal sector

A. Pedrera. *Instituto Geológico y Minero de España (IGME). a.pedrera@igme.es*
C. Marín-Lechado. *Instituto Geológico y Minero de España (IGME). c.marin@igme.es*

The sedimentary infill of the easternmost Almanzora Corridor and the western Huércal-Overa basin is deformed by ENE-WSW trending folds and reverse faults that sometimes affect the Quaternary sediments (e.g., Briend,1981; Soler et al., 2003; Masana et al., 2005; Pedrera et al., 2007). Folds have variable wavelengths (from meters to hundreds of meters) and geometries ranging from open to tight N-vergent with a minimum interlimb angle of 50°.

In the eastern Almanzora Corridor, between Partaloa and Urracal (Fig. 7.1). A prominent reverse fault is placed near Partaloa being in close spatial relation with these folds (Fig. 7.1). It has a slip greater than 40 m and produced the superposition of late Serravallian-lower Tortonian red conglomerates over upper Tortonian coral reefs. It is difficult to establish the activity of these structures during Quaternary times due to the absence of adequate deformation markers.

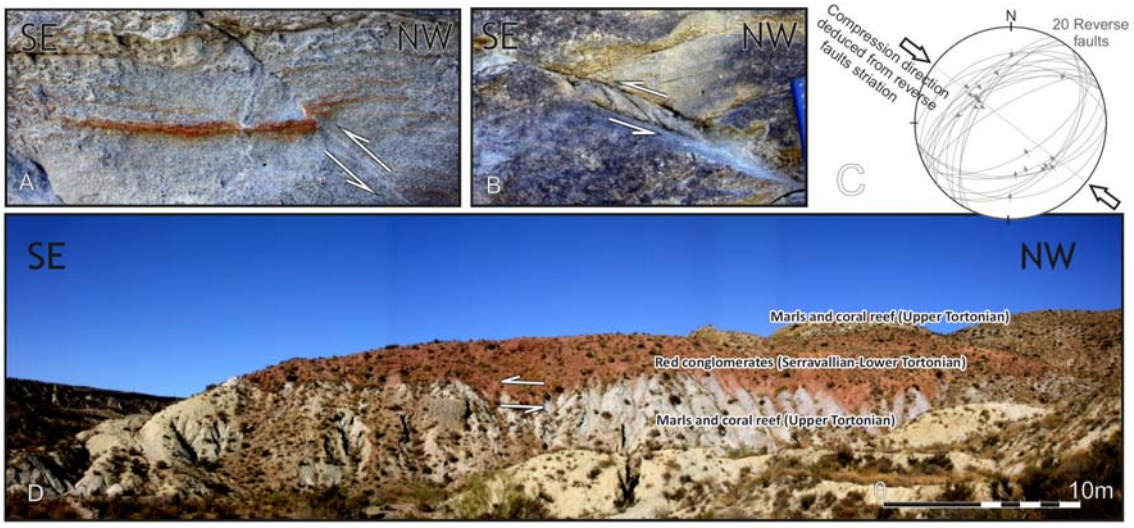

Fig. 7.1. Folds and reverse faults in the Partaloa-Urracal sector (Pedrera et al., 2007) (a, b) ENE-WSW reverse faults showing a few centimeter slips, in the central part of the basin. (c) Orientations and kinematics of 20 reverse faults plotted in a stereographic projection, lower hemisphere. Note that reverse faults have orientations from N45ºE to N90ºE, while the striations have directions comprised between N130ºE and N140ºE. (d) The main reverse fault of the study area has a maximum slip greater than 40 m, is located in the eastern sector, and favored the imbrication of lower Tortonian conglomerates over upper Tortonian coral reefs.

Stop 8. Fines Rambla (East of Urracal). Small scale active folds in the Partaloa–Urracal sector and quantitative geomorphic analyses

A. Pedrera. *Instituto Geológico y Minero de España (IGME). a.pedrera@igme.es*
C. Marín-Lechado. *Instituto Geológico y Minero de España (IGME). c.marin@igme.es*

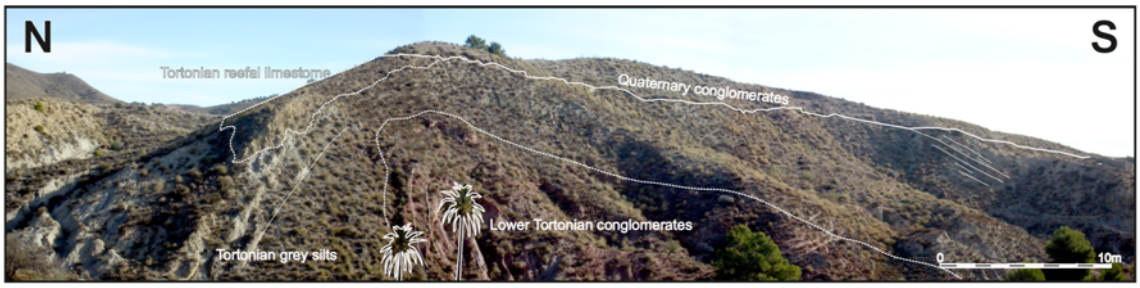

Figure 8.1. North-verging antiform in the Fines stream showing unconformity between lower and upper Tortonian units (Pedrera et al., 2009b).

The timing of the Partaloa-Urracal folds is deduced from the progressive unconformities. The dip increase from lower to upper Tortonian sediments is indicative of syn-tectonic sedimentation as could be observed across the Fines stream where the folds are well-exposed (Fig. 8.1). Quaternary alluvial fan deposits unconformably overlie the Miocene folded sequence, making it difficult to discern whether or not the folds affect or not the Quaternary rocks. This is due to the open geometry of the folds and the erosion in the alluvial fans by river incision.

Six longitudinal topographic profiles made along three alluvial fans developed on the northern Almanzora basin (A, B, and C, in Fig.8.2) allow us to infer the Quaternary folds activity. We analyzed the slope and differential erosion degree of alluvial fans A and B, located just over the folded Upper Miocene sediments, as well as the alluvial fan C, which is undisturbed by minor folds. The profiles were obtained picking the fan surfaces.

Since the fans are highly dissected, we have generated profiles envelopes by taking the topographic highs along the profiles that are related to the deformation caused by folds.

The two longitudinal profiles constructed along the alluvial fan A reveal two sectors. In the upper sector close to the apex, a flat partially eroded zone just coincides precisely with the antiform hinge (profile A2 in Fig. 8.2). Farther down, the fan reaches a normal and constant gradient (0.064). The three radial profiles made along the alluvial fan B show three different sectors: less-eroded upper and lower parts with a constant gradient (~0.033 for the three profiles) and a prominent more-eroded middle part. The same gradient is seen in the upper and the lower part of the alluvial fan, indicating a single fan generation. The elevated middle part of the profiles outlines the trace of the antiform. The profiles located over the alluvial fan C maintain a regular and constant gradient (0.044) throughout the profile and lacking any signs of deformation by folding.

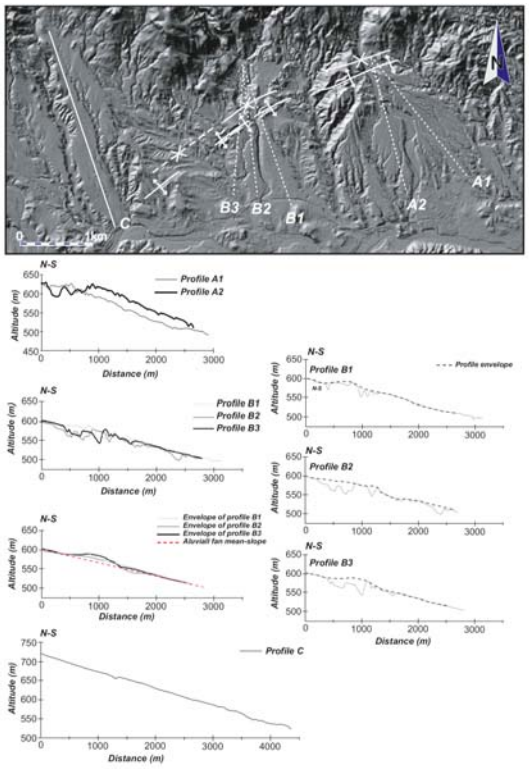

Figure 8.2. Enlarged image of the DEM (10-m grid) where is plotted the position of the alluvial fan and the topographic profiles (A and B) (Pedrera et al., 2009b). In order to better interpret the alluvial fan morphologies, we draw the envelope for the fan topographic profiles that show a clear elevated area in the three profiles that coincided to an antiform trace.

Quantitative geomorphic analysis

Active deformation structures have an incidence in topography that can be quantified by using geomorphic indices. The application of several

geomorphic indices (hypsometric curve analysis, normalized stream-length gradient, and valley width-to-valley height ratio) to the drainage network of the southern limb of the Sierra de Las Estancias antiform, where low-rate active folding has been recognized, allows us to investigate the suitability of these indices to identify active structures in such a scenario (Fig. 8.3).

River systems attain an erosion/sedimentation equilibrium characterized by slightly concave longitudinal profiles (Mackin, 1948; Schumm et al., 2000). Deviation from this river equilibrium profile may be induced by tectonic, lithological and/or climatic factors (Burbank and Anderson, 2000). The SLk index highlights anomalies in river longitudinal profiles, providing criteria to evaluate

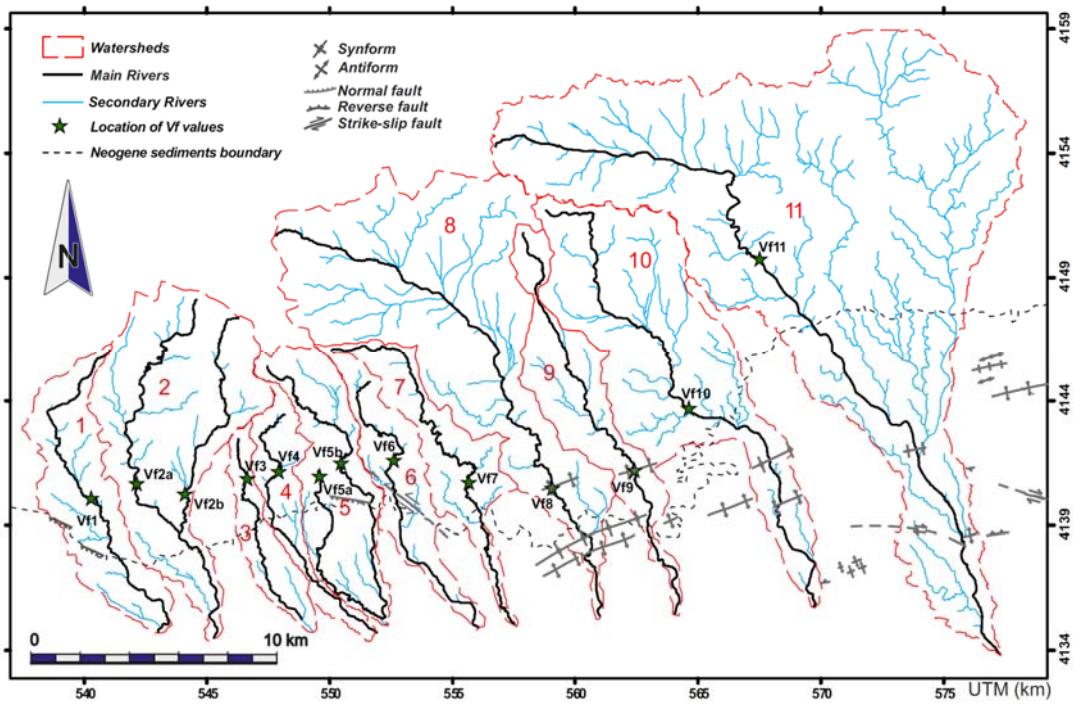

Figure 8.3. Position of the analyzed drainage network, the drainage basins, and the sectors where the Vf have been calculated (Pedrera et al., 2009b). The main active folds and faults are marked

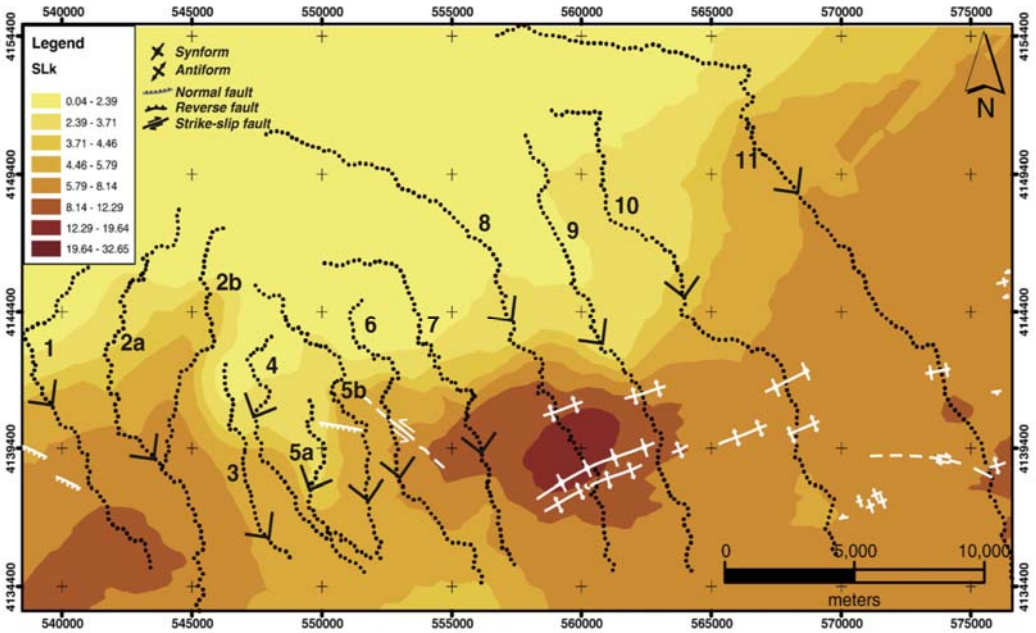

Figure 8.4. SLk anomaly map (Pedrera et al., 2009b).

and quantify these slope changes (Hack, 1973; Keller and Pinter, 2002; Pérez-Peña et al., 2009).
In order to assess the incidence of low rate active folds on channel equilibrium parameters we have performed stream-length gradient index (SLk) on the main tributary streams rivers. The anomaly map shows a local maximum over the metamorphic rocks of the Sierra de Las Estancias, which is detected on three rivers (rivers 7, 8, and 9 in Fig. 8.4). This maximum is elongated with an ENE–WSW trend, running parallel and coincident with the folds traces identified on the sediments. The Slk profiles of these rivers present two maximum values, which are displaced downstream from the topographic steps. In the other rivers studied, such SLk anomalies have were not detected, even though the rivers run from the hard metamorphic rocks of the Sierra de Las Estancias to the softer and more erodible Neogene sediments of the Almanzora Corridor.

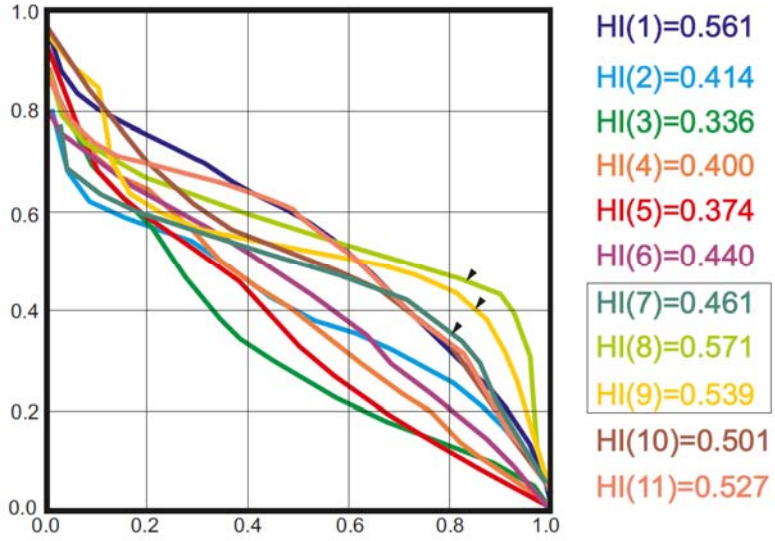

Figure 8.5. Hypsometric curves analyzed (Pedrera et al., 2009b). Curves corresponding to basins 7, 8, and 9, featuring convex shapes in the middle-mouth basin parts are marked (Modified from Pedrera et al., 2009b).

	Erd (m)	Hld (m)	Erd (m)	Vfw (m)	Vf
V_1	1053	1018	968	37	0.548
V_{2A}	1083	1134	978	164	1.257
V_{2B}	1000	1072	960	106	1.395
V_3	1087	1048	990	52	0.498
V_4	1055	1089	993	42	0.532
V_{5A}	1183	1110	1040	76	0.714
V_{5B}	887	952	785	35	0.260
V_6	1094	1027	946	30	0.262
V_7	1000	1014	875	14	0.106
V_8	1054	1120	790	15	0.050
V_9	1050	1075	769	20	0.068
V_{10}	860	779	713	95	0.892
V_{11}	919	859	746	105	0.734

Table 8.1. Vf values. Vf is the width of the valley; Erd and Eld are the elevations of the right and left valley divides respectively; Esc is the elevation of the valley floor (Pedrera et al., 2009b

Valley width to valley height ratio (Vf) (Bull and McFadden, 1977) is a geomorphic index conceived to discriminate between V-shaped valleys (Vf values close to 0) and U-shaped, flat-floored valleys (high Vf values). Deep V-shaped valleys are associated with linear active incision, distinctive of areas subjected to active tectonics; while flat floored valleys are characteristic of sectors with less river incision, where lateral erosion predominates in response to constant base levels and low tectonic activity (Keller and Pinter, 2002). The Vf values were obtained in the river reaches located above the rocks in order to avoid lithological controls, at a distance of ~1 km upstream from the contact between the basement and the sedimentary basins. We have calculated Vf

The hypsometric curve of a catchment represents the relative area below (or above) a given altitude (Strahler, 1952). These curves have been used to infer the stage of development of the drainage network, i.e., the erosional stage of the catchment (Keller and Pinter, 2002). Convex hypsometric curves characterize young slightly eroded regions; S-shaped curves characterize moderately eroded regions; concave curves point to old, highly eroded regions. The area below the hypsometric curve is known as the hypsometric integral (HI), varying from 0 to 1 (with values close to 0 in highly eroded regions and values close to 1 in slightly eroded regions).The hypsometric curves obtained for the 11 selected basins are shown in Fig. 23. We distinguished two groups with a particular curve shape. The basins located in the western sector (1, 2, 3, 4, 5, and 6) and the easternmost basins (10 and 11) constitute the first group, characterized by a general sub-rectilinear to very smooth concave–convex shapes. The second group corresponds to the basins in the eastern sector (basins 7, 8, and 9), featuring convex shapes in the middle-mouth basin parts. Therefore, the shape of the hypsometric curve also varies from catchments affected by active folding to those unaffected, though the precise location of the folds cannot be established.

The hypsometric curves of the catchments located in the folded sectors of the Sierra de Las Estancias-Almanzora basin are characterized by marked convex shapes in their middle-mouth sectors. These convex shapes are the result of the relative uplift caused by the folds

C³ References.

Andrieux, J., Fontbote, J.M., Mattauer, M. (1971). Sur un modele expiicatif de 1'Arc de Gibraltar. *Earth Planet. Sci. Lett.* 12, 191–198.

Argus, D. F., Gordon, R. G., DeMets, C., Stein, S. (1989). Closure of the Africa-Eurasia-North America plate motion circuit and tectonics of the Gloria fault. *J. Geophys. Res*. 94 : 5585–5602.

Augier R. (2004). Evolution tardi-orogénique des Cordilères Bétiques (Espagne): Apports d'un étude intégrée. PhD thesis, Université de Pierre et Marie Curie, Paris.

Baena, J., Ewert, K., (1982). Mapa Geológico de España 1/50.000, hoja n° 1058 (Roquetas de Mar). IGME. (in Spanish).

Booth-Rea, G., Azañón, J.M., Martínez-Martínez, J.M., Vidal, O., García-Dueñas, V., (2003). Análisis estructural y evolución tectonometamórfica del basamento de las cuencas neógenas de Vera y Huércal-Overa, Béticas orientales. *Revista de la Sociedad Geológica de España* 16: 193–209.

Bousquet JC, Montenat C. (1974). Présence de décrochements Nord-Est, Sud-Ouest plioquaternaires dans les Cordilléres bétiques orientales (Espagne). Extension et signification générale. *Comptes Rendus de l'Académie des Sciences* 278: 2617–2620.

Bousquet, J.C., Phillip, H. (1976). Observations microtectóniques sur la compresion nord-sud quaternaire des Cordillères bétiques orientales (Espagne meridionale-Arc de Gibraltar). *Bull Soc. Geol. France* 28, 711–724.

Briend M. (1981). Evolution morpho-tectonique du bassin néogéne de Huércal-Overa (Cordilléres bétiques orientales, Espagne). PhD thesis, Institut Geologique Albert de Lapparent, Paris.

Comas, M.C., García-Dueñas, V., Jurado, M.J. (1992). Neogene tectonic evolution of the Alborán Basin from MCS data. *Geo-Mar. Lett.* 12: 157-164.

Galindo-Zaldívar J, Gil AJ, Borque MJ, González-Lodeiro F, Jabaloy A, Marín-Lechado C, Ruano P, Sanz de Galdeano C. (2003). Active faulting in the internal zones of the central Betic Cordilleras (SE Spain). Journal of Geodynamics 36: 239–250.

Gràcia, E., Bartolome, R., Lo Iacono, C., Moreno, X., Stich, D., Martínez-Díaz, J.J., Bozzano, G., Martínez-Loriente, S., Perea, H., Diez, S., Masana, E., Dañobeitia, J.J.,Tello, O., Sanz, J.L., Carreño, E., EVENT-SHELF Team, (2012). Acoustic and seismicimaging of the Adra Fault (NE Alboran Sea): in search of the source of the 1910Adra earthquake. *Natural Hazards and Earth System Science* 12: 3255–3267.

Groupe de recherche Néotectonique de l'Arc de Gibraltar. (1977). L'histoire tectonique récente (Tortonien a` Quaternaire) de l'Arc de Gibraltar et des bordures de la mer d'Alboran. Bulletin de la Société Géologique de France 19: 575–614.

Guerra-Merchán A, Ramallo D, Ruiz Bustos A. (2001). New data on the Upper Miocene micromammals of the Betic Cordillera and their interest for marine–continental correlations. *Geobios* 34: 85–90.

Hack, J.T., 1973. Stream profile analysis and stream-gradient index. U.S. *Geological Survey Journal of Research* 1: 421–429.

Keller, E.A., Pinter, N., 2002. Active Tectonics. Earthquakes, Uplift, and Landscape. Prentice Hall, New Jersey.

Instituto Geográfico Nacional. (2008). http://www.ign.es/ [3 November 2008].

Lonergan, L., White, N. (1997). Origin of the Betic-Rif mountain belt. *Tectonics* 16: 504-522.

Mackin, J.H., 1948. Concept of the graded river. Geological Society of America Bulletin 59, 463–511.

Marín-Lechado, C., Galindo-Zaldívar, J., Rodríguez-Fernández, L. R., González-Lodeiro, F. (2004). Faulted hybrid joints: an example from the Campo de Dalías (Betic Cordilleras, Spain). *Journal of Structural Geology* 26: 2025–2037. doi:10.1016/j.jsg.2004.03.006

Marín-Lechado, C., Galindo-Zaldívar, J., Rodríguez-Fernández, L. R., Serrano I., Pedrera, A. (2005). Active faults, seismicity and stresses in an internal boundary of a tectonic arc (Campo de Dalías and Níjar, southeastern Betic Cordilleras, Spain). *Tectonophysics* 396: 81-96.

Marín-Lechado, C., A. Pedrera, J. A. Peláez, A. Ruiz-Constán, A. González-Ramón, and J. Henares (2017), Deformation style and controlling geodynamic processes at the eastern Guadalquivir foreland basin (Southern Spain), *Tectonics*, 36: doi:10.1002/2017TC004556.

Martínez-Díaz, J.J. (2002). Stress field variation related to fault interaction in a reverse oblique-slip fault: the Alhama de Murcia fault, Betic Cordillera, Spain. *Tectonophysics* 356: 291-305.

Martínez-Díaz, J.J., Hernández-Enrile, J.L. (2004). Neotectonics and morphotectonics of the southern Almería region (Betic Cordillera–Spain) kinematic implications. *Int. J. Earth Sci.* 93, 189-206. doi: 10.1007/s00531-003-0379-y.

Masana E, Martínez-Díaz JJ, Hernández-Enrile JL, Santanach P. (2004). The Alhama de Murcia fault (SE Spain), a seismogenic fault in diffuse plate boundary: seismotectonic implications for the Ibero-Magrebian region. *Journal of Geophysical Research* 109: 1–17.

Masana E, Pallàs R, Perea H, Ortuño M, Martínez-Díaz JJ, García-Meléndez E, Santanach P. (2005). Large Holocene morphogenic earthquakes along the Albox fault, Betic Cordillera, Spain. *Journal of Geodynamics* 40: 119–133.

Meijninger BML. (2006). Late-orogenic extension and strike-slip deformation in the Neogene of southeastern Spain. PhD thesis, Geologica Ultraiectina 269, University of Utrecht.

Mora M. (1993). Tectonic and sedimentary analysis of the Huércal-Overa region, SE Spain, Betic Cordillera. PhD thesis, University of Oxford.

Pedrera A, Galindo-Zaldívar J, Sanz de Galdeano C, López-Garrido AC. (2007). Fold and fault interactions during the development of an elongated narrow basin: the Almanzora Neogene–Quaternary Corridor (SE Betic Cordillera, Spain). *Tectonics* 26: TC6002.

Pedrera, A., Galindo-Zaldívar, J., Ruiz-Bustos, A., Rodríguez-Fernández, J., Ruíz- Constán, A. (2009a). The role of small-scale fold and fault development in seismogenic zones: example of the Western Huércal-Overa basin (Eastern Betic Cordillera, Spain). *J. Quat. Sci.* 24: 581–592, doi:10.1002/jqs.1246.

Pedrera, A., J. V. Pérez-Peña, J. Galindo-Zaldívar, J.M. Azañón, and A. Azor (2009b). Testing the sensitivity of geomorphic indices in areas of low-rate active folding (eastern Betic Cordillera, Spain). *Geomorphology* 105: 218–231.

Pedrera, A., Galindo-Zaldívar, J., Tello, A., Marín-Lechado, C. (2010a). Intramontane basin development related to contractional and extensional structure interaction at the termination of a major sinistral fault: The Huércal-Overa Basin (Eastern Betic Cordillera). *Journal of Geodynamics* 49: 271–286. doi:10.1016/j.jog.2010.01.008

Pedrera, A., Ruiz-Constán, A., Galindo-Zaldívar, J., Chalouan, A., Sanz de Galdeano, C., Marín-Lechado, C., Ruano, P., Benmakhlouf, M., Akil, M., López-Garrido, A.C., Chabli, A., Ahmamou, M., González-Castillo, L. (2011). Is there an active subduction beneath the Gibraltar orogenic arc? Constraints from Pliocene to present-day stress field. *Journal of Geodynamics* 52, 2, 83-96.

Pedrera, A., Galindo-Zaldívar, J., Marín-Lechado, C., García-Tortosa, F.J., Ruano, P., López-Garrido, A.C., Azañón, J.M., Peláez, J.A., Giaconia, F., (2012a). Recent and active faults and folds in the central–eastern internal zones of the Betic Cordillera. *Journal of Iberian Geology* 38: 191–208.

Pedrera, A., Marín-Lechado, C., Stich, D., Ruiz-Constán, A., Galindo-Zaldívar, J., Rey-Moral, C., Mancilla, F. (2012b). Nucleation, linkage and active propagation of a segmented Quaternary normal-dextral fault: the Loma del Viento fault (Campo de Dalías, Eastern Betic Cordillera, SE Spain). *Tectonophysics* 522–523: 208–217. doi: oi:10.1016/j.tecto.2011.12.001.

Pedrera, A., A. Ruiz-Constán, C. Marín-Lechado, J. Galindo-Zaldívar, A. González, and J. A. Peláez (2013). Seismic transpressive basement faults and monocline development in a foreland basin (Eastern Guadalquivir, SE Spain), *Tectonics* 32: 1571–1586, doi:10.1002/2013TC003397.

Pérez-Belzuz, F. (1999). Geología del Margen y Cuenca del Mar de Alborán durante el Plio-Cuaternario: Sedimentación y tectónica (PhD Thesis), University of Barcelona (538 pp.).

Pérez-Peña, J.V., Azañón, J.M., Azor, A., Delgado, J., González-Lodeiro, F., (2009). Spatial analysis of stream power using GIS: SLk anomaly maps. *Earth Surface Processes and* Landforms 34: 16–25.

Platt, J. P., S. Allerton, A. Kirker, A.Mandeville, C. Mayfield, E. S. Platzman, and A. Rimi (2003). The ultimate arc: differential displacement, oroclinal bending, and vertical axis rotation in the External Betic-Rif arc, *Tectonics* 22: 1017, doi 10.1029/2001TC001321.

Rodríguez-Fernández, J., Martín-Penela, J., (1993). Neogene evolution of the Campo de Dalías and surrounding offshore areas (Northeastern Alboran Sea). *Geodinamica Acta* 6: 255–270.

Sanz de Galdeano, C., Lopez Casado, C. (1988). Fuentes sísmicas en al ámbito Bético-Rifeño. *Rev. Geofis. Madrid* 44, 175-198.

Sanz de Galdeano C, López Casado C, Delgado J, Peinado MA. (1995). Shallow seismicity and active faults in the Betic Cordillera: a preliminary approach to seismic sources associated with specific faults. *Tectonophysics* 248: 293–302.

Schumm, S.A., Dumont, J.F., Holbrook, J.M., (2000). Active Tectonics and Alluvial Rivers. Cambridge University Press, Cambridge, UK. Burbank, D.W., Anderson, R.S., 2000. Tectonic Geomorphology. Blackwell Scientific, Oxford, UK. 270 pp.

Soler R, Masana E, Santanach P. (2003). Evidencias geomorfológicas y estructurales del levantamiento tectónico reciente en la terminación sudoccidental de la falla de Alhama de Murcia (Cordillera Bética Oriental). *Revista de la Sociedad Geológica de España* 16: 123–133.

Strahler, A.N., (1952). Hypsometric (area–altitude) analysis of erosional topography. *Geological Society of America Bulletin* 63: 1117–1142.

Stich D, Serpelloni E, Mancilla F, Morales J. (2006). Kinematics of the Iberia–Maghreb plate contact from seismic moment tensors and GPS observations. *Tectonophysics* 42: 295–317.

Vázquez, J.T., (2001). Estructura del Margen Continental septentrional del Mar de Alborán (PhD Thesis). Universidad Complutense de Madrid, Facultad de Ciencias Geológicas, Departamento de Geodinámica, p. 422.

Vernant, P., Fadil, A., Mourabit, T., Ouazar, D., Koulali, A., Davila, J.M., Garate, J., McClusky, S., Reilinger, R.E. (2010). Geodetic constraints on active tectonics of the Western Mediterranean: implications for the kinematics and dynamics of the Nubia-Eurasia plate boundary zone. *J. Geodyn.* 49: 123–129, doi:10.1016/j.jog.2009.10.007.

Wilkins, S.J., Gross,M.R., Wacker,M., Eyal, Y., Engelder, T., (2001). Faulted joints kinematics, displacement–length scaling relations and criteria for their identification. *Journal of Structural Geology* 23: 315–327.

Zazo, C., Goy, J.L., Dabrio, C.J., Bardají, T., Hillaire-Marcel, C., Ghaleb, B., González-Delgado, J.A., Soler, V., (2003). Pleistocene raised marine terraces of the Spanish Mediterranean and Atlantic coasts: records of coastal uplift, sea-level highstands and climate changes. *Marine Geology*: 194, 103–133.

C³ Cuadernos de Campo del Cuaternario Vol., 3. 2016. AEQUA, Almería. 23 pp.

Pedrera A, Martín Lechado, C. Eds (2016). *Quaternary Tectonics in the Huercal-Overa and Eastern Basins of Almería (Eastern Betic Cordillera, SE Spain)*